

# Development and characterisation of conductive knitted fabrics as humidity sensors for automatic hemostasis detection

DOI: 10.35530/IT.076.06.202536

EMILIA VISILEANU  
ALEXANDRA GABRIELA ENE  
RAZVAN RADULESCU

FELICIA DONDEA  
LAURENTIU DINCA  
ADRIAN SALISTEAN

## ABSTRACT – REZUMAT

### Development and characterisation of conductive knitted fabrics as humidity sensors for automatic hemostasis detection

Conductive knitted fabrics can function as humidity sensors, detecting the presence of liquids on their surface through changes in electrical resistance. This property can be leveraged for automatic hemostasis systems, where the detection of blood at a wound site triggers real-time intervention. In this study, conductive yarns including Shieldex (Statex: 60-440  $\Omega/m$ ), AgSiS (Lib-40: 5  $\Omega/m$ ), and stainless steel (60  $\Omega/m$ ) were integrated into knitted fabrics using a Shima Seiki machine. The fabrics were characterised for mechanical strength, abrasion resistance (1,000 and 5,000 cycles), washing durability (1 and 5 cycles), and resistance to acidic and alkaline perspiration. Electrical resistance was measured under exposure to four aqueous media simulating physiological and wound conditions: deionised water (pH 6, 244  $\mu S/cm$ ), acidic perspiration (pH 5.5, 10.73 mS/cm), alkaline perspiration (pH 8, 11.35 mS/cm), and 20% saline solution (pH 5.0, 9.5 mS/cm). Morphological and compositional analyses were conducted using SEM, EDX, and FTIR spectroscopy. The results demonstrated that all fabrics exhibited measurable and repeatable resistance variations, with the strongest response observed for the 20% saline solution and Lib-40 conductive yarn, highlighting their potential as humidity sensors for real-time detection of bleeding events in automatic hemostasis systems.

**Keywords:** conductive textiles, knitted fabrics, humidity sensor, automatic hemostasis system, electrical resistance monitoring, combat garment

### Dezvoltarea și caracterizarea structurilor textile tricotate conductive ca senzori de umiditate pentru detectarea automată a hemostazei

Structurile tricotate conductive pot funcționa ca senzori de umiditate, detectând prezența lichidelor pe suprafața lor prin modificări ale rezistenței electrice. Această proprietate poate fi utilizată în sisteme automate de hemostază, în care detectarea sângelui la nivelul unei răni declanșează o intervenție în timp real. În acest studiu, fire conductoare, inclusiv Shieldex (Statex: 60-440  $\Omega/m$ ), AgSiS (Lib-40: 5  $\Omega/m$ ) și oțel inoxidabil (60  $\Omega/m$ ), au fost integrate în structuri tricotate utilizând o mașină Shima Seiki. Tricoturile au fost caracterizate din punct de vedere al rezistenței mecanice, rezistenței la abraziune (1.000 și 5.000 cicluri), durabilității la spălare (1 și 5 cicluri) și rezistenței la transpirație acidă și alcalină. Rezistența electrică a fost măsurată în condiții de expunere la patru medii apoase care simulează condiții fiziologice și de rană: apă deionizată (pH 6, 244  $\mu S/cm$ ), transpirație acidă (pH 5,5, 10,73 mS/cm), transpirație alcalină (pH 8, 11,35 mS/cm) și soluție salină 20% (pH 5,0, 9,5 mS/cm). Analizele morfologice și compoziționale au fost realizate utilizând SEM, EDX și spectroscopie FTIR. Rezultatele au demonstrat că toate tricoturile conductive au prezentat variații măsurabile și repetabile ale rezistenței electrice, cea mai puternică reacție fiind observată pentru soluția salină 20% și firul conductiv Lib-40, evidențiind potențialul acestora ca senzori de umiditate pentru detectarea în timp real a sângerărilor în sistemele automate de hemostază.

**Cuvinte-cheie:** tricoturi conductive, senzor de umiditate, sistem automat de hemostază, detectarea sângerării, monitorizarea rezistenței electrice, îmbrăcăminte combatanți

## INTRODUCTION

Smart textiles are capable of converting environmental stimuli, such as temperature, light, chemical composition, humidity, or pH, into measurable physical or aesthetic responses through mechanical and electromagnetic interactions. Over the past decades, these systems have evolved from rigid electronics mounted

on fabrics to fully textile-based, flexible, adaptive, and biomimetic solutions (figure 1) [1, 2].

Typically, smart textiles comprise a fabric substrate, conductive interconnectors, sensors, actuators, energy sources, and processing units, with conductivity introduced at various stages, such as during polymerisation, fibre spinning, fabric construction, or post-processing via coating or printing (figure 2).

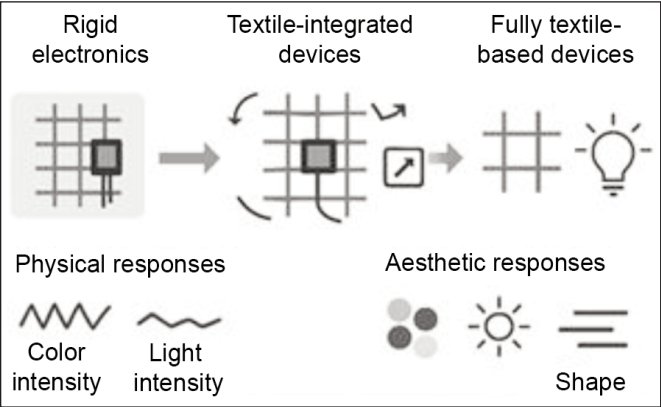


Fig. 1. Schematic illustrating the evolution of smart textiles from rigid electronics to a fully textile-based adaptive system

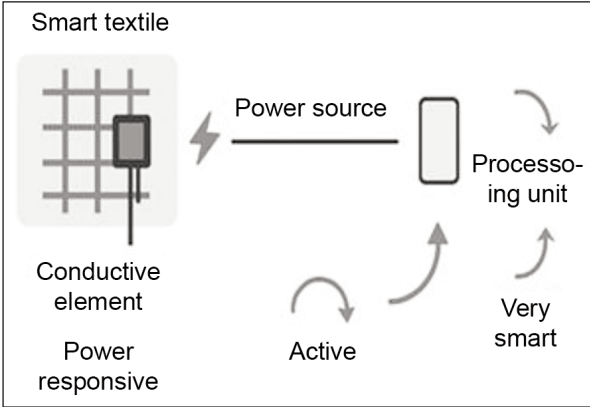


Fig. 2. Components of a smart textile system and classification according to interaction

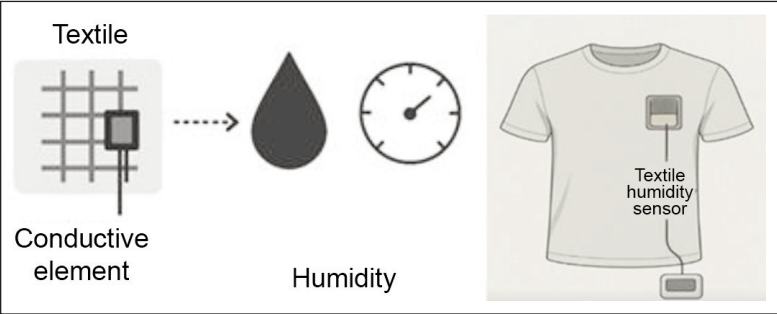


Fig. 3. Textile-based humidity sensor integrated into a wearable patch for real-time monitoring of moisture and physiological parameters [5]

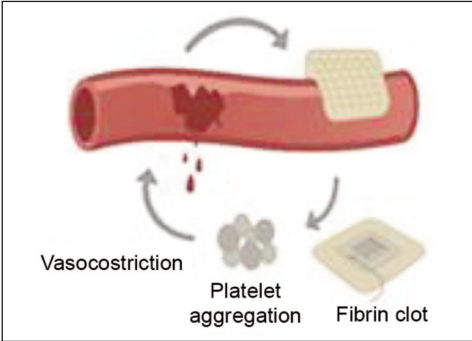


Fig. 4. Schematic representation of physiological hemostasis

Conductive additives, including metals, carbon-based fillers, graphene, nanotubes, and conductive polymers, enable electrical functionality but may influence mechanical resilience and durability. Textile-integrated sensors, fabricated at the fibre, yarn, or fabric level using knitting, weaving, embroidery, or layered structures, exploit these conductive elements to measure mechanical deformation, pressure, strain, or environmental stimuli [3, 4]. Among these applications, humidity-sensitive textiles are particularly relevant in biomedical contexts, providing critical physiological information through real-time monitoring of moisture, sweat, or wound exudates (figure 3) [5, 6].

In hemostasis, rapid detection of local moisture associated with blood or exudate can provide essential feedback on the effectiveness of dressings and interventions. Hemostasis is the physiological process that prevents and stops bleeding following vascular injury, involving vascular constriction, platelet plug formation, and coagulation to form a stabilising fibrin clot (figure 4) [7, 8]. Pathological conditions or impaired coagulation may necessitate medical intervention, highlighting the need for rapid detection systems. Conductive textiles, capable of detecting changes in electrical resistance caused by contact with blood or body fluids, can serve as sensors for automatic hemostasis systems, triggering control signals for wound management or alerting medical personnel [9, 10]. Recent work on textile-based wound dressings has demonstrated that changes in fluid presence (blood, exudate) can be detected using conductive or capacitive fabrics [11]. Similarly, textile biosensors for

sweat and other body fluids have shown that smart fabrics can reliably monitor physiological moisture changes in real time [12, 13]. One recent example embedded a protein sensor into a fabric dressing for wound healing monitoring [14, 15]. In this study, we investigate the electrical and mechanical behaviour of several conductive knitted fabrics under exposure to fluids simulating blood and body perspiration, evaluating their potential as humidity sensors for real-time bleeding detection in automatic hemostasis systems (figure 5). Due to safety and regulatory constraints,

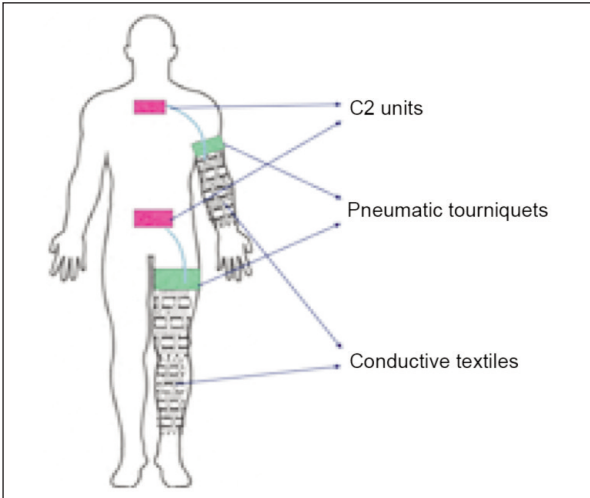


Fig. 5. Schematic representation of the automatic hemostasis system [16]

blood simulants were used; future work will include real blood testing for calibration.

## GENERAL INFORMATION

### Conductive yarns

The selection of conductive yarns was based on a set of electrical, mechanical, and material-related criteria. The linear resistance  $R_L$  ( $\Omega/\text{m}$ ) was first considered, as it represents a key electric parameter. The electric conductivity of the yarns  $\sigma$  [ $\text{S}/\text{m}$ ] is computed based on the linear resistance  $R_L$  and the optical diameter  $D$  (equation 1) (for the length of the yarn  $L = 1 \text{ m}$ ):

$$\sigma = \frac{1}{R_L} \frac{L}{\frac{\pi}{4} D^2} \quad (\text{S}/\text{m}) \quad (1)$$

Young's modulus  $E$  was calculated by the ratio between the stress  $\sigma$  ( $\text{N}/\text{m}^2$ ) and the strain  $\varepsilon$  (%) (2):

$$E = \frac{\sigma}{\varepsilon}, \quad \sigma = \frac{F}{A}, \quad \varepsilon = \frac{\Delta L}{L_0} \quad (2)$$

where  $F$  is breaking force (N),  $A$  – the cross-sectional area of the wire ( $\text{m}^2$ ),  $L_0$  – initial length (m), and  $\Delta L$  – elongation (m).

### Knitted fabrics

Conductive fabrics were manufactured using knitting technology with conductive yarns, including Shieldex 2-Ply HC+B TPU, Shieldex Ply (STATEX), Sprinox (Ugitec), and DA 5359 (FILIX), whose physical, mechanical, and electrical properties were systematically assessed. Knitting was performed on Shima Seiki SIR 122G07 and 122G14 flat knitting machines. Figure 6 presents the technical programming drawing to create a knitting component (a sleeve) along with the main design parameters. An intarsia-type structure was produced using metallic yarn combined with Nm 50/1 cotton yarn, featuring 8-needle cotton borders. The knitted fabric measured 412 courses in length and 256 courses in width, with a stitch size of 5.3 mm (figure 6, a). The fabric was knitted in a sequence of 2 rows of metallic yarn alternating with 4 rows of cotton yarn (Nm 50/2), creating a conductive textile structure. Border of 6 needles using BBC-type yarn, row 122 GO7, knit length – 170 loops, maximum width – 128 loops, stitch – 10.8 mm (figure 6, b).

### Characterisation methods of the fabrics

Given that these conductive knitted fabrics are intended for combatants, it is essential to evaluate their performance under realistic operational condi-

tions. Abrasion tests assess mechanical durability under repeated friction and stress, ensuring the sensor maintains functionality during intense physical activity. Sweat tests, including both acidic and alkaline perspiration, simulate physiological conditions that may influence electrical response, verifying that the sensors remain accurate without false triggers. Air permeability tests ensure that the fabrics are breathable and comfortable when integrated into wearable combat gear. Finally, washing tests evaluate the durability of the textiles under repeated cleaning cycles, confirming that the electrical and mechanical properties are preserved for long-term use in the field. Together, these evaluations guarantee that the conductive fabrics can reliably function as humidity sensors for automatic hemostasis detection while withstanding the demanding conditions faced by soldiers.

Tensile strength was tested according to SR EN ISO 13935-1:2013 using a Titan Universal Strength Tester (strip method, 50 mm specimen width,  $200 \pm 1 \text{ mm}$  gauge length, 20 mm/min speed). Abrasion resistance was assessed following SR EN ISO 12947-2:2016 with a Martindale 404 tester under a load of 12 kPa and total effective mass of  $795 \pm 7 \text{ g}$ , using standardised abrasive fabric and Lissajous motion. Washing durability was examined in accordance with SR EN ISO 105-C06:2010 on a GIRO HW-Jams Heal washing machine ( $40^\circ\text{C}$ , 30 min, 4 g/l ECE detergent without optical brighteners, 150 ml washing liquid). Resistance to acidic and alkaline perspiration was determined following SR EN ISO 105-E04:2013. SEM imaging revealed the surface morphology of the conductive textiles after durability tests, while EDX confirmed their elemental composition. FTIR analysis identified both organic and inorganic compounds present in the materials.

Four wetting media were prepared for the conductive textile structures: tap water, acidic perspiration (pH 5.5), alkaline perspiration (pH 8), and 20% saline solution. For safety and ethical reasons, blood simulants (saline and perspiration solutions) were used to reproduce the ionic and moisture characteristics of real blood. Future validation will include calibration with standardised blood simulants to confirm the detection thresholds under real biological conditions. Acidic and alkaline perspiration were prepared according to SR EN ISO 105-E04, using L-histidine hydrochloride, NaCl, and phosphate salts, with pH adjusted using 0.1 M HCl or NaOH. The saline solution was prepared at 20 g NaCl/l.

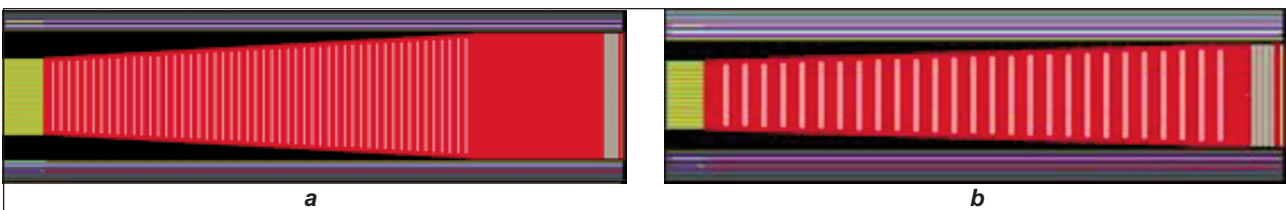


Fig. 6. Screenshots of the structures: a – intarsia-type structure; b – conductive textile structure





Fig. 7. The measurement area



Fig. 8. Bullet imprint

Conductive textile structures were tested for performance using 10 ml of liquid, a 5s wetting time, and a 5 cm diameter test area (figure 7). Electrical resistance measurements were carried out, taking into account, as much as possible, the need to maintain the same length of the conductive yarn, despite the high elasticity of the material. Particular attention was given to the variation of the electrical resistance of each knitted structure under the four moisture conditions, as well as to the limits within which these values fall, to be correlated with the activation parameters of the primary hemostasis system control unit. The electrical resistance [ $\Omega$ ] was measured for the textiles in three conditions: initial, after wetting, and after wetting in a moulded “bullet imprint” (figure 8). The bullet imprint simulates localised mechanical deformation and micro-wetting caused by penetration, reflecting realistic conditions when a combatant experiences a bleeding wound. Measurements were taken using a Multimeter of type FLUKE 179, capable of measuring  $0.1 \Omega$  to  $\geq 50 \text{ M}\Omega$ .

## RESULTS AND DISCUSSION

The conducted experiments aimed to determine how conductive knitted fabrics respond electrically and mechanically to the presence of blood-simulating liquids and perspiration, to evaluate their suitability for integration into an automatic hemostasis system. Variations in electrical resistance under different wetting conditions (water, saline, acidic, and alkaline sweat) were analysed to establish the sensitivity and stability of the textile sensors in realistic physiological environments.

The following types of yarns were selected to manufacture the knitted fabrics: Shieldex 2-Ply HC+B TPU, Shieldex Ply (STATEX), Sprinox (Ugitech), and DA 5359 (FILIX). The physical-mechanical and electric properties are presented in table 1.

The diameter and cross-sectional area of the wires strongly influence mechanical behaviour, user comfort, and the feasibility of integration into textile structures. While thicker yarns provide lower resistance, they are less flexible and more difficult to conceal within fabrics, whereas thinner yarns are easier to embed but may be prone to breakage under mechanical stress. In addition, the composition and surface

plating of the yarns (e.g., copper, silver-plated copper, stainless steel, or nickel–chromium alloys) were considered, as these factors not only affect conductivity and resistance to oxidation but also determine cost-efficiency and biocompatibility. Therefore, the chosen set of yarns reflects a balance between electrical performance, mechanical durability, and practical suitability for integration into conductive textiles.

The physical-mechanical properties of the manufactured knitted samples are presented in table 2.

All fabrics maintained structural integrity and electrical performance after 1,000 and 5,000 abrasion cycles, confirming suitability for combat use.

Abrasion testing ensures that blood detection remains reliable even under friction or stress. Fabrics exhibited measurable changes in resistance depending on pH, but signals remained detectable, showing reliable performance under body-fluid exposure. Knitted fabrics were sufficiently breathable, allowing moisture and air transport without compromising sensor function. Electrical and mechanical properties were largely preserved after 1 and 5 wash cycles, confirming that fabrics can withstand operational maintenance.

The following electric resistance results were collected during the wetting of the knitted fabrics with various types of droplets (table 3).

Figure 9 compares the resistance of each conductive textile structure across different conditions: initial, surface water-treated, and water-treated within the bullet imprint, simulating localised penetration.

A logarithmic y-axis was used to accommodate the wide range of values, from very low to very high (e.g., t11)

The presence of the water causes an increase in electrical resistance for all treated textile structures (t10 > 9.9%; t12: > 6.5%; t13: > 16%) except t11, which remains at the same level (70.8 k $\Omega$  and 68.7 k $\Omega$ ). In the case of the bullet imprint, electrical resistance decreases for all variants, with the largest reductions observed for variants t10 (< 42.0%) and t11 (< 100%); t12: < 45% except t13, which records an increase (t13 > 9.%)

The presence of acidic perspiration (conductivity: 37.2 mS/cm and pH-5.5) results in an increase in the resistance values of the treated textile structures: t10 > 2.5%; t11: 7.7%; t12: 14.5%; t13 > 11.4%. In variants t11 and t12, significant increases in electrical

Table 1





PHYSICAL-MECHANICAL AND ELECTRIC PROPERTIES OF CONDUCTIVE YARNS						
No.	Properties / Yarn type	Unit	Shieldex 2-Ply HC+B TPU(Statex)	Shieldex Ply(Statex)	Sprlnox (Ugitech)	DA5393 Ecrú (Filix)
						
1	Fibrous composition	%	PA6.6/Ag-99.9%		Spun yarn	30% metal / 70% PES
2	Linear density	Tex (Nm)	15x2 (66.6/2)	14.0x2 (71.42/2)	89x2 (11.2/2)	12.67x2 (78.93/2)
		Dtex (Den)	152x2 (136.8x2)	140x2 (126x2)	890x2 (801x2)	126.7x2 (139.3x1)
	CV	%	0.38	0.83	3.63	1.89
3	Breaking strength	N	13.40	1348.30	1734.35	6.67
		Cv%	3.28	1.48	10.01	4.15
4	Breaking elongation	%	26.35	25.89	1.25	18.89
		Cv%	6.64	2.46	5.12	11.15
5	Elasticity moduls (E)	GPa	1.13	27.9	13.01	-
6	Twist fibres	T/m	643.2	620	232	28.4
		Cv%	0.49	0.68	4.90	9.85
7	Torque	-	Z	S	Z	Z
8	Twist yarn	T/m	587.2	560	138	629.6
		Cv%	2.58	0.86	2.02	6.04
9	Torque	-	S	Z	S	S
10	Linear electric resistance	$\Omega$ /m	150	440	60	940
11	Optical diameter	$\mu$ m	240	248	412	160
12	Electric conductivity	S/m	146991	46930	124698	52776

Table 2

PHYSICAL-MECHANICAL PROPERTIES OF CONDUCTIVE KNITTED FABRICS								
No	Properties		Unit	Results/variants				Standard
				T10 – Shieldex PLY (Statex)	T11 – DA 5393 (FILIX)	T12 – 2HC-PLY (Statex)	T13 – Sprlnox (Ugitech)	
1	Specific mass		g/m²	153.6	158.4	170.4	263.0	SR EN12127:2003
2	Yarns density	Warp	No yarns/ 10 cm	76	70	70	40	SR EN 1049-2:2000, Method A,B
		Weft		96	110	100	50	
3	Thickness		mm	0.92	0.8	0.95	1.20	SR EN ISO 5084:2001
4	Air permeability		l/m²/s	3496	3258	3222	4192	SR EN ISO 9237:1999
5	Breaking force	V	N	254.22	284.22	227.54	73.2	SE EN ISO 13934-1/2013
		H		108.69	125.17	153.60	70.43	
6	Elongation at break	V	%	47.31	49.53	52.05	18,6	SE EN ISO 13934-1/2013
		H		67.91	62.67	80.86	24.15	
7	Elasticity modulus (E)	V	MPa	11.7	14,34	9.1	6.56	-
		H		3.46	5.00	4.0	4.86	
8	Abrasion resistance	1000	Cycles	No broken stitches	No broken stitches	No broken stitches	Stitches broken at 1500 cycles	SR EN ISO 12947-2/2017
		5000						

resistance are observed in the bullet imprint (t11: from 68  $\Omega$  to 169  $\Omega$ ; t12 from 172.9  $\Omega$  to 600  $\Omega$ ). In these cases, the bullet impact may damage or compress conductive pathways, creating microcracks.

Also, acidic sweat can corrode or oxidise metallic or conductive coatings, reducing connectivity. Localised moisture can dissolve ions into insulating residues, increasing resistance. For the other textile structures,

Table 3

FABRIC USED FOR THE EXPERIMENTS							
No	Wet environment	State	T10 – Shieldex PLY (Statex)	T11 – DA 5393 (FILIX)	T12 – 2HC-PLY (Statex)	T13 – Sprlnox (Ugitech)	Observation
1	Water, pH=5.5, C=688 $\mu$ S/cm, Quantity: 5 ml	Initial	171 $\Omega$	70.8 k $\Omega$	214 $\Omega$	89.9 $\Omega$	T = 27.90°C RH = 25.0%
		Treat	188 $\Omega$	68.7 k $\Omega$	228 $\Omega$	105.4 $\Omega$	
		Bullet print	71.8 $\Omega$	0.9 $\Omega$	98.4 $\Omega$	98.8 $\Omega$	
2	Acid sweat, pH=5.5, C=37.2 mS/cm, Quantity: 5 ml	Initial	198.3 $\Omega$	68.7 $\Omega$	179.2 $\Omega$	220.3 $\Omega$	T = 31.40°C RH = 27.3%
		Treat	203.1 $\Omega$	74 $\Omega$	260 $\Omega$	252.1 $\Omega$	
		Bullet print	109 $\Omega$	169 k $\Omega$	600 $\Omega$	110 $\Omega$	
3	Alkaline sweat, pH=8.0, C=24.7 mS/cm, Quantity: 5 ml	Initial	108.5 $\Omega$	10 $\Omega$	86.3 $\Omega$	147.5 $\Omega$	T = 34.50°C RH = 28.0%
		Treat	104.6 $\Omega$	8.52 $\Omega$	99.8 $\Omega$	142.8 $\Omega$	
		Bullet print	61.5 $\Omega$	30.7 $\Omega$	97.6 $\Omega$	155 $\Omega$	
4	Saline solution, pH=5.0, C=27.4 mS/cm, Quantity: 5 ml	Initial	104.8 $\Omega$	11.6 $\Omega$	105.3 $\Omega$	123.3 $\Omega$	T = 29.10°C RH = 29.4%
		Treat	98.3 $\Omega$	9.8 $\Omega$	104.8 $\Omega$	116.8 $\Omega$	
		Bullet print	99.7 $\Omega$	2.1 $\Omega$	36.3 $\Omega$	115.0 $\Omega$	

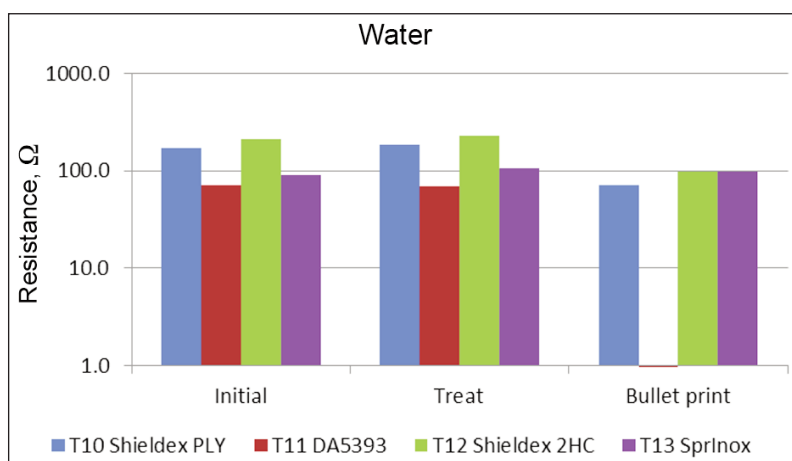


Fig. 9. Electrical resistance of conductive structures: initial, water-treated, and bullet-imprint states

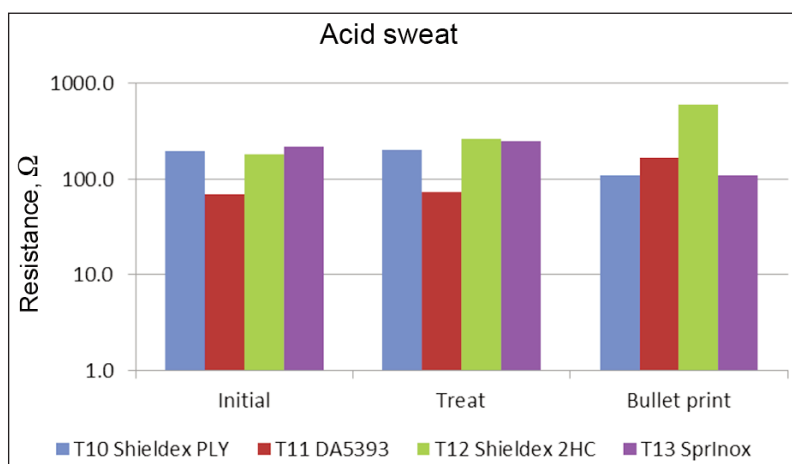


Fig. 10. Electrical resistance of conductive structures: initial, acid sweat, treated, and bullet-imprint states

electrical resistance at the bullet-imprint state, values are lower compared to the initial state: t10 109  $\Omega$  versus 198  $\Omega$ , and t13 110  $\Omega$  versus 220  $\Omega$ . In these cases, acidic sweat can act as a temporary ionic conductor, providing additional pathways for current.

The presence of alkaline perspiration (conductivity: 24.7 mS/cm, pH=8) generally reduces the electrical resistance of treated textile structures: t10 < 3.8%; t11 < 1.17%; and t13 < 0.96%. For the textile structure t12 (Shieldex 2HC), a slight, insignificant increase in resistance is observed (1.13%).

Alkaline perspiration functions as a temporary ionic conductor, leading to a decrease in electrical resistance in most cases. However, the Shieldex yarn (2HC), due to its complex structure, is more sensitive to alkaline exposure, resulting in a minor increase in resistance, likely due to possible oxidation. In the case of the bullet imprint, electrical resistance increases for most variants (t11 > 100%; t12 > 12.4%; t13 > 6%) and decreases for variant t10 (< 44%). Alkaline sweat can corrode or oxidise metallic or conductive coatings, reducing connectivity.

The presence of the saline solution (20% concentration, conductivity 27.4 mS/cm, pH 5) causes a decrease in electrical resistance for all treated textile structures (t10 < 6.8%; t11 < 16%; t12 < 1%; t13 < 6%). In the case of the bullet imprint, electrical resistance decreases for all variants, with the largest reductions observed for variants t11 (DA 5393 yarn) and t12 (Shieldex 2HC yarn) (t10 < 5%; t11 < 72%; t12 < 64%; t13 < 7%).

Saline solutions contain dissolved ions ( $\text{Na}^+$ ,  $\text{Cl}^-$ ). When the solution contacts the textile, these ions create additional conductive pathways along the fibres. Essentially, the textile's effective

conductivity increases because the current can move through the ionic solution as well as the textile's own conductive elements. This is why electrical resistance drops across all treated textile variants.

Correlation analysis between the thread's linear electric resistance ( $\Omega/\text{m}$ ) and the woven fabric's total resistance ( $\Omega$ ) under each test condition and state was calculated. The graphical representation of the correlation between thread linear resistance and fabric sample resistance under each condition and state is presented in figure 14.

High correlations ( $|r| > 0.9$ ) indicate that the linear resistance of the thread has a strong influence on the overall fabric resistance, but the direction (positive or negative) changes depending on the environment and the type of damage. Positive correlations (e.g., Water Initial, Acid Bullet): higher-resistance threads lead to higher overall fabric resistance. Negative correlations (in most other cases): suggest that lower-resistance threads yield higher fabric resistance, likely due to better conductivity pathways or interaction effects when the threads are immersed or damaged. After bullet damage, correlations often flip in sign or weaken, implying that structural damage alters the current distribution and reduces the predictable relationship between the thread's intrinsic resistance and the fabric's overall resistance.

These correlations indicate that resistance changes are detectable and predictable, providing reliable triggers for an automatic hemostasis control system. The FTIR spectrum exhibits a characteristic band at  $550\text{ cm}^{-1}$  corresponding to silver oxide (t10), indicating oxidation of the silver surface, likely caused by atmospheric moisture [16]. SEM analysis shows that the initial fibre samples are morphologically clean. EDS analysis reveals oxygen and carbon originating from the polymeric filament support of the silver film, with additional oxygen attributed to silver oxide. After perspiration and washing tests, a slight increase in oxygen concentration is observed, attributable to reactions between silver and oxygen. The t11 sample, composed solely of polymeric components, displays FTIR peaks characteristic of organic functional groups [17]. SEM images show minor surface degradation after perspiration and washing, particularly following five wash cycles. EDS confirms carbon and oxygen elements typical of organic polymers.

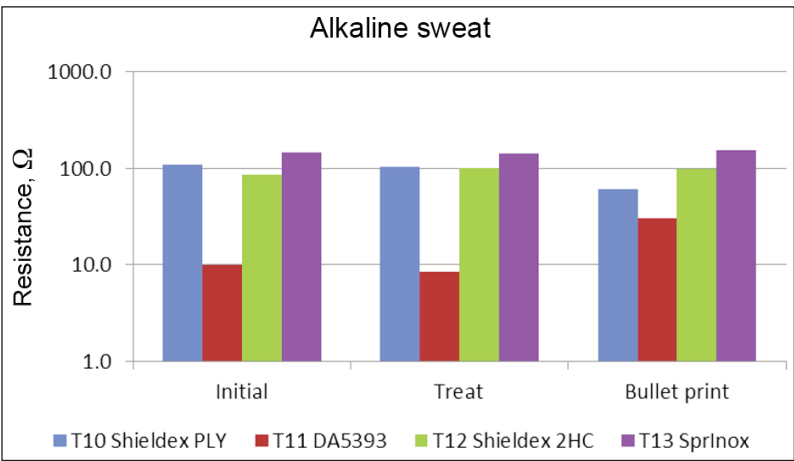


Fig. 11. Electrical resistance of conductive structures: initial, alkaline sweat-treated, and bullet-imprint states

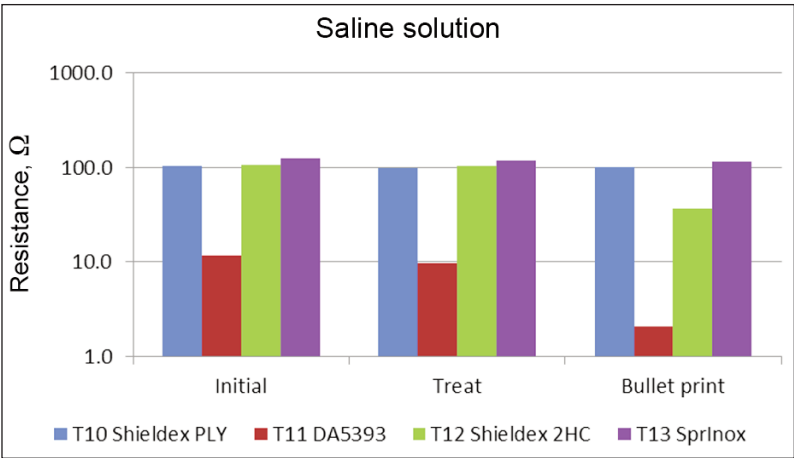


Fig. 12. Electrical resistance of conductive structures: initial, saline solution-treated, and bullet-imprint states

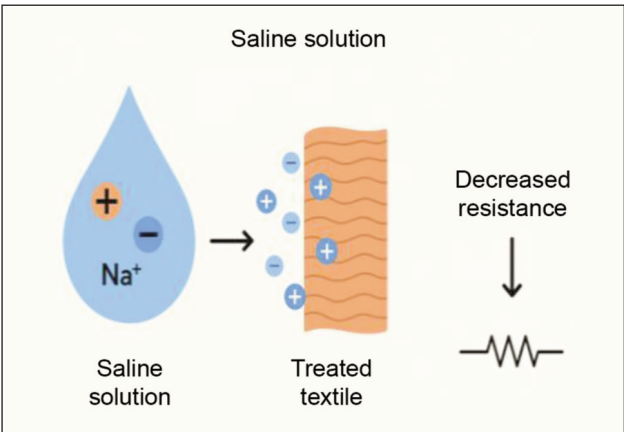


Fig. 13. Illustration of the physical principle

For sample t12, the spectral band at  $550\text{ cm}^{-1}$ , assigned to silver oxide lattice vibrations, is evident, again indicating oxidation, possibly due to ambient humidity. SEM micrographs reveal an almost clean fibre surface, while EDS results confirm oxygen and carbon contributions from both the polymeric support and silver oxide. Samples subjected to perspiration and washing show slight oxygen increases, consistent with the high reactivity of silver toward oxidation.



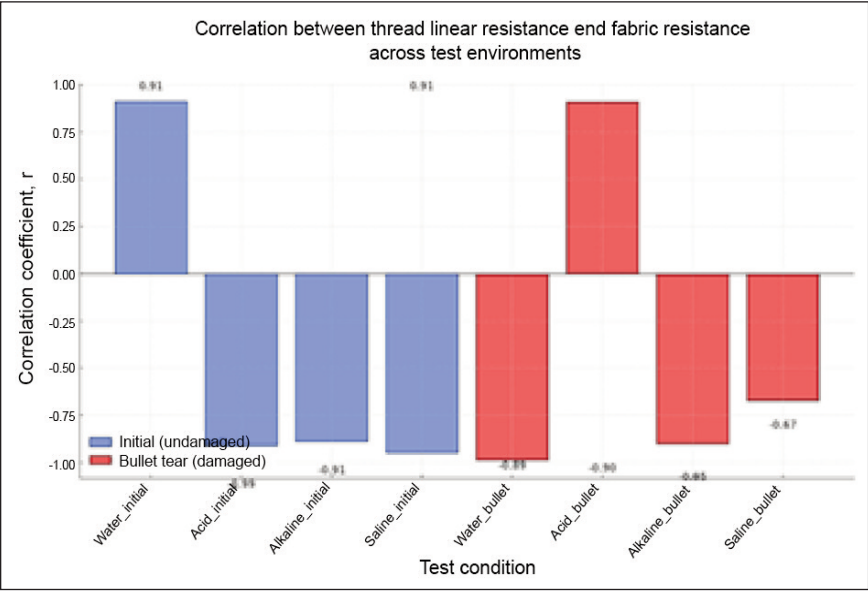
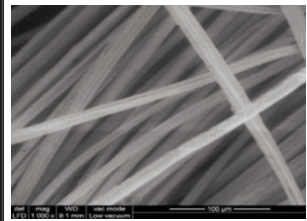
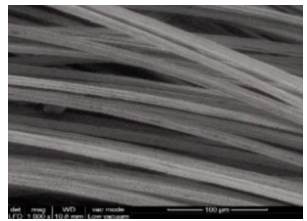
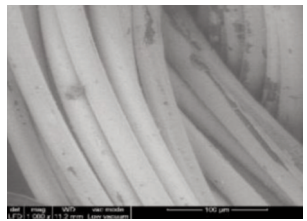
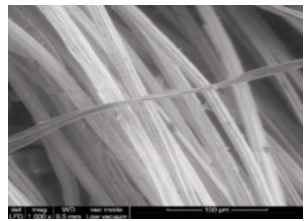


Fig. 14. Correlation between thread linear resistance and fabric sample resistance

Table 4 presents SEM micrographs and elemental data for variant t13 in the initial state and after exposure to acidic and alkaline perspiration and five washing cycles. The spectral bands at 465, 551, 1628, and 3450  $\text{cm}^{-1}$ , characteristic of iron oxides, are absent, indicating that the iron surface remains unoxidized (figure 15). SEM images show a clean surface, and EDS detects oxygen and carbon associated with the polymeric support. Only the sample washed five times exhibits a minor oxygen increase, suggesting trace amounts of iron oxide formed through limited reaction with water.

Table 4

SEM IMAGES																																																																																			
1000xSEM image and element concentration – Initial	1000xSEM image and element concentration – Acid perspiration	1000xSEM image and element concentration – Alkaline perspiration	1000xSEM image and element concentration – Washing (5 cycles)																																																																																
																																																																																			
<table border="1"> <thead> <tr> <th>Element</th><th>Weight %</th><th>Atomic %</th><th>Error %</th></tr> </thead> <tbody> <tr> <td>CK</td><td>3.9</td><td>14.6</td><td>35.4</td></tr> <tr> <td>OK</td><td>3.5</td><td>9.8</td><td>20.2</td></tr> <tr> <td>CrK</td><td>20.5</td><td>17.7</td><td>17.5</td></tr> <tr> <td>FeK</td><td>72.1</td><td>58.0</td><td>14.5</td></tr> </tbody> </table>	Element	Weight %	Atomic %	Error %	CK	3.9	14.6	35.4	OK	3.5	9.8	20.2	CrK	20.5	17.7	17.5	FeK	72.1	58.0	14.5	<table border="1"> <thead> <tr> <th>Element</th><th>Weight %</th><th>Atomic %</th><th>Error %</th></tr> </thead> <tbody> <tr> <td>CK</td><td>5.0</td><td>18.2</td><td>30.1</td></tr> <tr> <td>OK</td><td>3.5</td><td>9.6</td><td>20.4</td></tr> <tr> <td>CrK</td><td>19.9</td><td>16.7</td><td>18.5</td></tr> <tr> <td>FeK</td><td>71.5</td><td>55.6</td><td>13.7</td></tr> </tbody> </table>	Element	Weight %	Atomic %	Error %	CK	5.0	18.2	30.1	OK	3.5	9.6	20.4	CrK	19.9	16.7	18.5	FeK	71.5	55.6	13.7	<table border="1"> <thead> <tr> <th>Element</th><th>Weight %</th><th>Atomic %</th><th>Error %</th></tr> </thead> <tbody> <tr> <td>CK</td><td>8.1</td><td>27.5</td><td>20.0</td></tr> <tr> <td>OK</td><td>2.2</td><td>5.6</td><td>30.2</td></tr> <tr> <td>CrK</td><td>19.7</td><td>15.5</td><td>17.4</td></tr> <tr> <td>FeK</td><td>70.1</td><td>51.4</td><td>12.8</td></tr> </tbody> </table>	Element	Weight %	Atomic %	Error %	CK	8.1	27.5	20.0	OK	2.2	5.6	30.2	CrK	19.7	15.5	17.4	FeK	70.1	51.4	12.8	<table border="1"> <thead> <tr> <th>Element</th><th>Weight %</th><th>Atomic %</th><th>Error %</th></tr> </thead> <tbody> <tr> <td>CK</td><td>8.0</td><td>25.9</td><td>21.8</td></tr> <tr> <td>OK</td><td>5.3</td><td>12.9</td><td>15.0</td></tr> <tr> <td>CrK</td><td>17.9</td><td>13.3</td><td>15.0</td></tr> <tr> <td>FeK</td><td>68.8</td><td>47.9</td><td>12.7</td></tr> </tbody> </table>	Element	Weight %	Atomic %	Error %	CK	8.0	25.9	21.8	OK	5.3	12.9	15.0	CrK	17.9	13.3	15.0	FeK	68.8	47.9	12.7
Element	Weight %	Atomic %	Error %																																																																																
CK	3.9	14.6	35.4																																																																																
OK	3.5	9.8	20.2																																																																																
CrK	20.5	17.7	17.5																																																																																
FeK	72.1	58.0	14.5																																																																																
Element	Weight %	Atomic %	Error %																																																																																
CK	5.0	18.2	30.1																																																																																
OK	3.5	9.6	20.4																																																																																
CrK	19.9	16.7	18.5																																																																																
FeK	71.5	55.6	13.7																																																																																
Element	Weight %	Atomic %	Error %																																																																																
CK	8.1	27.5	20.0																																																																																
OK	2.2	5.6	30.2																																																																																
CrK	19.7	15.5	17.4																																																																																
FeK	70.1	51.4	12.8																																																																																
Element	Weight %	Atomic %	Error %																																																																																
CK	8.0	25.9	21.8																																																																																
OK	5.3	12.9	15.0																																																																																
CrK	17.9	13.3	15.0																																																																																
FeK	68.8	47.9	12.7																																																																																

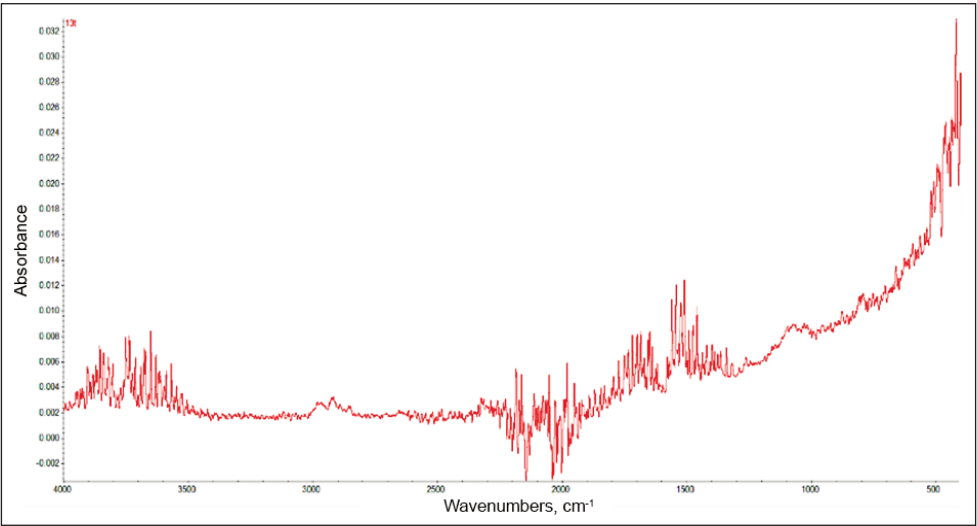


Fig. 15. FT-IR spectrum



## RELEVANCE TO HEMOSTASIS DETECTION

The results demonstrate that conductive textiles can serve as functional sensors for detecting the presence of conductive fluids such as blood. During an injury, when a bullet or sharp object pierces the fabric, the contact of blood with the conductive textile alters its electrical resistance, which can be immediately detected by a control unit. This change acts as a trigger for an automatic hemostasis system, capable of initiating wound-sealing mechanisms or sending alerts to medical personnel.

The experimental findings show that:

- Electrical resistance decreases significantly upon contact with saline or blood-like fluids due to increased ionic conductivity.
- The “bullet imprint” condition simulates the localised wetting and mechanical deformation caused by penetration, confirming that the resistance change is strong enough to be used as a detection signal.
- Acidic and alkaline sweat tests demonstrate that body fluids influence sensor performance; however, the conductive pathways remain functional, confirming the textiles’ potential reliability under physiological conditions.

Therefore, the conductive knitted fabrics analysed in this study can be integrated as moisture and blood-detection sensors in protective garments, providing the essential feedback component for an automatic hemostatic control system.

## CONCLUSIONS

This study demonstrates the feasibility of using conductive knitted fabrics as humidity and blood sensors for integration into automatic hemostasis systems. The electrical resistance of the fabrics changes measurably upon contact with liquids, including saline and body-fluid simulants, providing a reliable detection mechanism for bleeding events.

Key findings include:

- Electrical response: All fabric variants showed significant resistance changes upon wetting, with the largest response observed for 20% saline solution, confirming sensitivity to conductive fluids similar to blood.
- Mechanical performance: Fabrics maintained integrity and consistent sensor performance after abrasion and washing cycles, demonstrating durability for wearable combat applications.
- Chemical stability: SEM, EDX, and FTIR analyses revealed minor oxidation in silver-coated yarns, while stainless steel variants remained stable, ensuring sensor reliability.
- Environmental influence: Acidic and alkaline perspiration affected resistance differently, but all fabrics maintained detectable signal changes, confirming robustness under physiological conditions.
- Application relevance: These resistance variations can serve as triggers for an automatic hemostasis control unit, enabling real-time intervention in bleeding events.

In conclusion, the conductive knitted fabrics studied here function effectively as humidity sensors capable of detecting blood or wound moisture, providing a reliable basis for automatic hemostasis systems. Changes in electrical resistance under bullet-imprint and fluid exposure provide clear signals that can trigger automatic hemostasis control units, enabling real-time intervention during bleeding events. Future work will focus on calibration with blood simulants, integration with electronic control units, and optimisation of signal thresholds for field applications.

## ACKNOWLEDGEMENTS

This work was supported by a grant of the ANC, CCDI-UEFISCDI, project number PN-IV-P7-7.1-PED-2024-0353, within PNCDI IV.

## REFERENCES

- [1] Júnior, H.L.O., Neves, R.M., Monticeli, F.M., Dall Agnol, L., *Smart Fabric Textiles: Recent Advances and Challenges*, In: Textiles, 2022, 2, 4, 582–605, <https://doi.org/10.3390/textiles2040034>
- [2] Sajovic, I., Kert, M., Boh Podgornik, B., *Smart Textiles: A Review and Bibliometric Mapping*, In: Applied Sciences, 2023, 13, 18, 10489, <https://doi.org/10.3390/app131810489>
- [3] Ruckdashel, R.R., Khadse, N., Park, J.H., *Smart E-Textiles: Overview of Components and Outlook*, In: Sensors, 2022, 22, 16, 6055. <https://doi.org/10.3390/s22166055>
- [4] Li, X., Wang, Q., Zheng, L., Xu, T., *Smart Janus textiles for biofluid management in wearable applications*, In: iScience, 2024, 27, 3, 109318, ISSN 2589-0042, <https://doi.org/10.1016/j.isci.2024.109318>
- [5] Winterhalter, C.A., Teverovsky, J., Wilson, P., Slade, J., Horowitz, W., Tierney, E., Sharma, V., *Development of electronic textiles to support networks, communications, and medical applications in future U.S. military protective clothing systems*, In: IEEE Trans Inf Technol Biomed., 2005, 9, 3, 402–406, <https://doi.org/10.1109/titb.2005.854508>
- [6] Liu, F., Hong, J., Chen, X., et al., *Ultrafast humidity sensor and transient humidity detections in high dynamic environments*, In: Commun Eng, 2025, 4, 4, <https://doi.org/10.1038/s44172-025-00342-4>
- [7] Alzahrani, H., Okmi, A., Florence, S.S., Ishak, K.A., Bin Mamat M.H., Roslan, N.A., Supangat, A., *Sensitivity enhancement of NPD: Alq3-based organic humidity sensor via thermal annealing treatment*, In: Sensors and Actuators A: Physical, 2025, 95, 117085, ISSN 0924-4247, <https://doi.org/10.1016/j.sna.2025.117085>
- [8] Çelenk, E., Tokan, N.T., *All-Textile On-Body Antenna for Military Applications*, In: IEEE Antennas and Wireless Propagation Letters, 2022, 21, 5, 1065–1069, <https://doi.org/10.1109/LAWP.2022.3159301>

- [9] Holland Stephen, A., *Conductive Textiles and their use in Combat Wound Detection, Sensing, and Localization Applications*, Master's Thesis, University of Tennessee, 2013, [https://trace.tennessee.edu/utk\\_gradthes/1627](https://trace.tennessee.edu/utk_gradthes/1627)
- [10] Vazquez-Garza, E., Jerjes-Sanchez, C., Navarrete, A. et al., *Venous thromboembolism: thrombosis, inflammation, and immunothrombosis for clinicians*, In: J Thromb Thrombolysis, 2017, 44, 377–385
- [11] Pötzschke, et al., *Monitoring of Surgical Wounds with Purely Textile, Measuring Wound Pads – III: Detection of Bleeding or Seroma Discharge by the Measurement of Wound Weeping*, In: Textiles, 2022, 2, 4, 546–559, <https://doi.org/10.3390/textiles2040031>
- [12] Akter, A., et al., *Recent Studies on Smart Textile-Based Wearable Sweat Sensors for Medical Monitoring: A Systematic Review*, In: Journal of Sensor and Actuator Networks, 2024, 13, 4, 40, <https://doi.org/10.3390/jsan13040040>
- [13] Olaru, S., Filipescu, E., Filipescu, E., Niculescu, C., Salistean, A., *Software solution to assess morphological body through 3D scanning results*, In: Proceedings of the 9th International Scientific Conference eLearning and software for Education Bucharest, April 25–26, 2013, 3, ISSN 2066-026X, 391–398
- [14] Akter, A., et al., *Development of a textile-based protein sensor for monitoring the healing progress of a wound*, In: Scientific Reports, 2022, 12, 1, 7972, <https://doi.org/10.1038/s41598-022-11982-3>
- [15] Patent no. RO 133698. *Autonomous System for Primary Hemostasis*
- [16] Murtaza, A., Zaheeruddin, K., *Synthesis and FTIR Characterization of Iron Oxide Nanoparticles*, In: IJIRSET, 2019, 8, 3, 2963–2965, <https://doi.org/10.15680/IJIRSET.2019.0803219>,
- [17] Rafiq, M., Siddiqui, H., Adil, S.F., Assal, M.E., Roushoun, A., AL-Warh, A., *Synthesis and Characterization of Silver Oxide and Silver Chloride Nanoparticles with High Thermal Stability*, In: Asian Journal of Chemistry, 2013, 25, 6, 3405–3409

---

**Authors:**

EMILIA VISILEANU, ALEXANDRA GABRIELA ENE, RAZVAN RADULESCU, FELICIA DONDEA,  
LAURENTIU DINCA, ADRIAN SALISTEAN

National Research and Development Institute for Textiles and Leather  
16, Lucretiu Patrascanu street, district 3, code 030508, Bucharest, Romania

**Corresponding author:**

EMILIA VISILEANU  
e-mail: [e.visileanu@incdtp.ro](mailto:e.visileanu@incdtp.ro)